Periodico di Mineralogia (2013), 82, 1, 1-23 DOI: 10.2451/2013PM0001

PERIODICO di MINERALOGIA
established in 1930

An International Journal of
MINERALOGY, CRYSTALLOGRAPHY, GEOCHEMISTRY, ORE DEPOSITS, PETROLOGY, VOLCANOLOGY
and applied topics on *Environment*, *Archaeometry* and *Cultural Heritage*

Geochemical characteristics of Kanigorgeh ferruginous bauxite horizon, West-Azarbaidjan province, NW Iran

Ali Abedini*[,1] and Ali Asghar Calagari[2]

[1]Department of Geology, Faculty of Sciences, University of Urmia, 57153165, Urmia, Iran
[2]Department of Geology, Faculty of Natural Sciences, University of Tabriz, 5166616471, Tabriz, Iran
*Corresponding author: *abedini2020@yahoo.com* and *a.abedini@urmia.ac.ir*

Abstract

Ferruginous bauxite horizon of Kanigorgeh is located ~ 20 km northeast of Bukan, West-Azarbaidjan province, northwest Iran. The horizon is a part of the Irano-Himalayan karst bauxite belt that was developed in a form of 8 discontinuous stratified layers and lenses varying in thicknesses (5-17 m) with extending over 3.2 km along the contact of Permian carbonates, Triassic dolomites. In this study, parental affinity and controlling factors of elements distribution in the bauxite ores are surveyed by applying analytical mineralogy, mass and volume changes calculations (method of isocon), elemental ratios, and correlation coefficients. Mineralogical analyses reveal that diaspore, hematite, and kaolinite are the major minerals in the ores with lesser and variable amounts of boehmite, goethite, muscovite-illite, rutile, and montmorillonite. In contrast to the presence of diasporic-boehmitic mineralogical composition in ores, the geochemical data (i.e., ratios of Pb/Y, Ga/Pb, Zr/Pb, and Cr/Ni), testify to gibbsitic composition for the original aluminum hydroxides. Microscopic studies and geochemical characteristics of major and trace elements indicate that the ores were formed authigenically by the alteration and weathering of basaltic parent rocks. Mass change calculations suggests that enrichment of many elements in the ores resulted by losing Si, Ca, K, Na, Mg, and P during weathering of plagioclase, K-feldspar, ferromagnesians, and apatite. In addition, variable amounts of Co, Sr, and Ba were lost during bauxitization. Geochemical considerations prove that distribution of major, minor, trace, and rare earth elements in the studied ores were principally controlled by factors such as cation exchanges, adsorption, increasing of pH in weathering solutions due to buffering by carbonate bedrocks, scavenging by Fe-oxides and hydroxides, isomorphic substitutions, co-precipitation, and differences in stability of primary minerals.

Key words: Bauxite; Parent rock; Mass changes; Elemental distribution; Kanigorgeh; Iran.

Introduction

Bauxites are rocks enriched in Al, Ga, and REEs (Calagari and Abedini, 2007; Liu et al., 2010). They can be ores of these metals, but also are mined for concentrations of Ni, Au, Nb, and P (Freyssinet et al., 2005; Retallack, 2010). From geological point of view, bauxites are residual rocks that formed intermittently throughout much of the geologic record during periods of intense continental subaerial weathering (Meyer, 2004).

Bauxite deposits can be classified into two main categories, depending on the bedrock lithology: (1) the one which is overlying aluminosilicate rocks and (2) another which is overlying carbonate rocks. According to Bardossy (1982), bauxites are overlying aluminosilicate rocks can be further subdivided into (1) laterite bauxites (consisting of residual deposits and/or deposits that experienced only local redeposition) and (2) Tikhvin-type bauxites representing transported (allochthonous) deposits without showing any perceptible relationship with the original residual profile. Bauxites that are lying on carbonate rocks can be categorized as "karstic", regardless of whether the bedrock surface is karstified or not, or the degree of karstification. Based on morphology, composition, and geographical-paleogeographical criteria, the bauxite deposits are classified into six groups, (1) Mediterranean-type, (2) Timan-type, (3) Kazakhstan-type, (4) Ariege-type, (5) Salento-type, and (6) Tulsk-type. Based upon geographic distribution, they occur in seven belts throughout the world, (1) northern Mediterranean coast, (2) Caribbean basin, (3) Ural-Siberia-Central Asia, (4) Eastern Asia, (5) Irano-Himalaya, (6) Southwestern Pacific, and (7) Northern America (Bardossy, 1982). The geochemistry of Irano-Hymalayan bauxite belt was less noted by researchers. Some geochemical works had been done on this belt and the results were published (e.g., Calagari and Abedini, 2007; Zarasvandi et al., 2008, 2010; Calagari et al., 2010; Esmaeili et al., 2010). These studies showed that these bauxite deposits are very similar to Mediterranean type karst bauxite.

Ferruginous bauxite deposit at Kanigorgeh is a typical Permo-Triassic residual horizon on this belt in northwest Iran. No geochemical studies on this horizon have been done so far. In this study, we endeavore to combine the data that is obtained from field work, petrography, analytical mineralogy, and geochemistry (elemental ratios, mass and volume change calculations, and correlation coefficients) and then to characterize the parental affinity and factors that they are controlling the distribution of major, minor, trace, and rare earth elements in this deposit.

Geological framework

Regional geology

The bauxite horizons of Kanigorgeh are located ~ 20 km northeast of Bukan, West-Azarbaidjan province, NW Iran. In the structural domains classification of Iran, they are a part of Sanandaj-Sirjan zone (Figure 1a). In this zone, Permian limestone underwent several depositional cessations by epirogenic movements during upper Permian (Kamineni and Efthekhar-nezad, 1977). The entire Iranian platform was affected by these movements which were accompanied locally by basic volcanic activities especially in Alborz mountain chain. These eruptive basic volcanic rocks are cropped out in many locations in northwest Iran (Kamineni and Efthekhar-nezad, 1977; Calagari and Abedini, 2007) including studied area (at Kanigorgeh). As a result of upper Permian epirogenic movements, major uplift took place which was followed by marine regression from a vast region along NW-SE trending belt in Iran. Lateritization occurred after each uplift event that was repeated several times during the formation of Permian limestone.

During late Triassic to early Jurassic time the Paleozoic platform in the west of Iran (separated structurally from the central Iranian platform)

sank and a deep trough was developed which was filled by thick Jurassic-Cretaceous sediments. These sediments are present in northwest of Iran (Kamineni and Efthekhar-nezad, 1977). During Laramide movements the Sanandaj-Sirdjan structural zone was established and the rocks underwent strong deformation and/or regional metamorphism, accompanied by magmatism (Kamineni and Efthekhar-nezad, 1977). These geologic events are believed to have affected the laterites. Some of these laterites, due to bauxitization processes were partially converted into bauxite. Bauxitization process of laterites in Sanandaj-Sirjan structural zone of Iran was implemented by factors such as deferrugenization-ferrugenization, desilisification, and fluctuation of underground water table level.

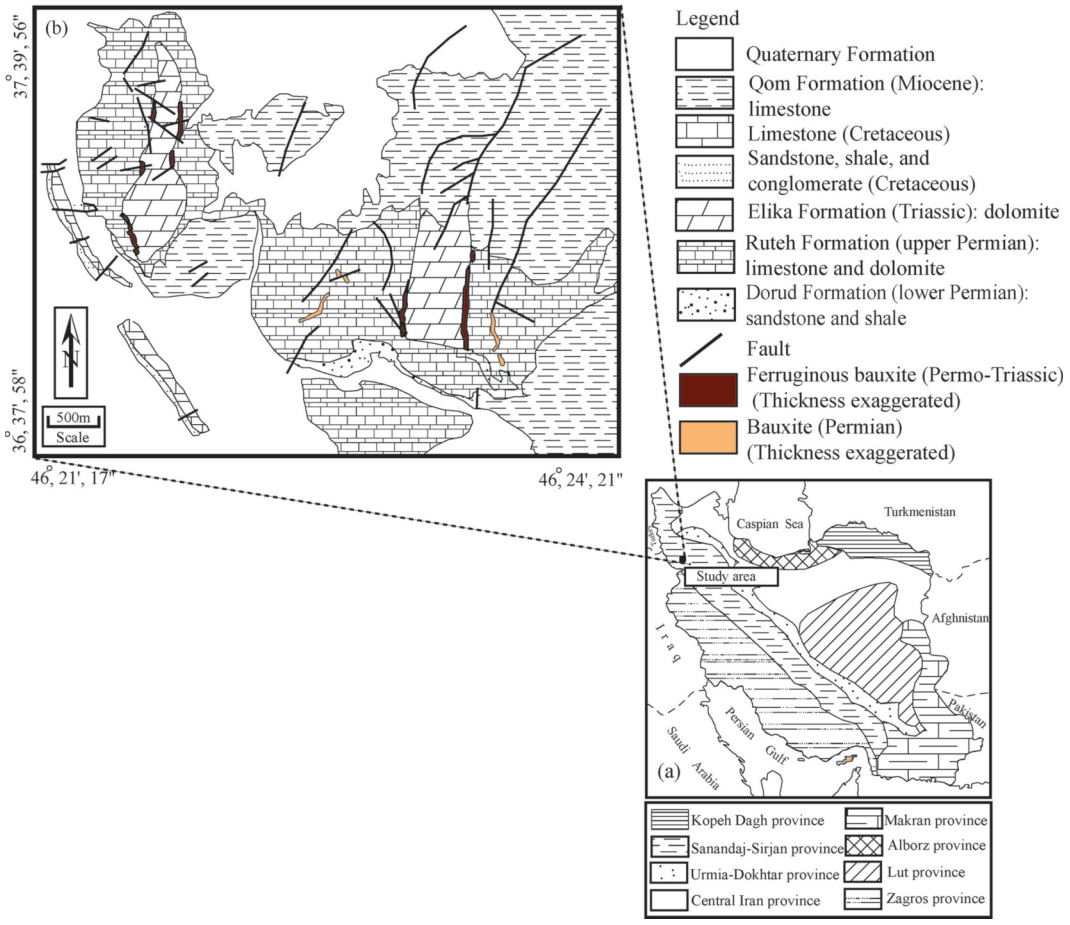

Figure 1. a) An index map of Iran showing the eight structural zones. Also the location of study area on the Sanandaj-Sirdjan structural zone is shown on this map (modified after Vaziri-Moghaddam et al., 2006). b) Geological map illustrating the position of bauxitic layers and lenses at Kanigorgeh.

Geology of the deposit

The major lithologic units in studied area, from the oldest to the youngest, are lower Permian sandstone and shale; upper Permian limestone and dolomite; Triassic dolomite; Cretaceous sandstone, shale, and conglomerate; Cretaceous limestone; Miocene limestone, and Quaternary alluvial sediments (Figure 1b). The bauxite ores in this area occurred in two distinct horizons. The first one has rather limited extent and consists of 4 discontinuous stratified layers and/or lenses trending NW-SE, NE-SW, and N-S directions within the upper Permian carbonate rocks (Figure 1b). They are extended over 1 km with varying thickness ranging from 2 to 11 meters. The second one is vastly spread and is developed along the border of upper Permian carbonate rocks and Triassic dolomite. It consists of 8 discontinuous stratified layers and/or lenses trending NW-SE and N-S directions, extending over 3.2 km with varying thickness ranging from 5 to 17 meters. The bauxite ores in both horizons with their enclosing rocks suffered structural stresses and were severely folded. The activity of faults caused the development of cataclastic texture within the layers and/or lenses. Bauxitic ores were occasionally and partially limonitized by supergene oxidizing solutions. The remnants of partially altered basaltic rocks in the form of irregular patches were also observed in the contact of the bedrocks and Permo-Triassic bauxite horizon. The bedrocks adjacent to the contact in many places were turned into pink to purple color as the result of gradual diffusion of Fe-bearing solutions into existing interstices. Irregular joints related to dynamic stress were developed in bauxitic layers and lenses. Furthermore, it seems that the bauxites were developed chiefly on the cavities, depressions, and karstic sinkholes of the bedrocks. The Permo-Triassic bauxite ores display two distinct forms, massive and stratified. They show various colors including red, dark red, and brownish red. Compared to the stratified, the massive ores are denser and were mainly developed adjacent to the carbonate bedrock.

Some notable geological features of the Permo-Triassic bauxite horizon include the sharp contact between bauxite ores and enclosing rocks; the presence of mesoscopically observable nodes, ooids and occasionally pisoids in the ores; and the existence of dendritic Mn-oxides in the ores. Some ores have soapy, greasy, and earthy feels while others are hard and massive with conchoidal fracture surfaces.

Materials and methods

On the basis of field relations, 80 ore samples from 8 layers and lenses of Permo-Triassic bauxite and 5 samples from basaltic rocks that are existing in the contact of the ores and carbonate bedrocks, were collected. After mesoscopic examination, 23 samples of the bauxitic ores and 2 samples of the basaltic rocks were selected for mineralogical and geochemical studies. Thin and thin-polished sections of these selected samples were prepared and then tested under microscope. The mineralogical composition of 12 selected samples were semi-quantitatively determined by using X-ray diffraction (SIEMENS Diffractometer, Model D-5000, CuKα radiation, fixed graphite chromators, voltage 40kV, current 40 mA, scanning speed 2° per minute, scan range 2-70°, drive axis 2Θ) in Geological Survey of Iran. Finally, all 25 selected samples were chemically analyzed in Acme analytical Laboratories (Vancouver, Canada). The compositional values of major and minor oxides along with the trace and rare earth elements were determined by using ICP-MS method. The LOI (Loss on ignition) values were measured on the basis of weighting the samples before and after one hour of heating at 1000 °C. The results of chemical analyses along with detection limits are listed in Table 1.

Results

Petrography

Microscopic observations exhibited that the basaltic rocks (existing in the contact of bauxitic ores with carbonate bedrocks) possess porphyritic, hyalo-microlitic porphyry, and intersertal textures. Mineralogically, these rocks mainly contain phenocrysts of plagioclase (Figure 2a) and ferromagnesian minerals set in a microlitic matrix of plagioclase, K-feldspar, epidote, calcite, sericite, tremolite, apatite, augite, biotite, and

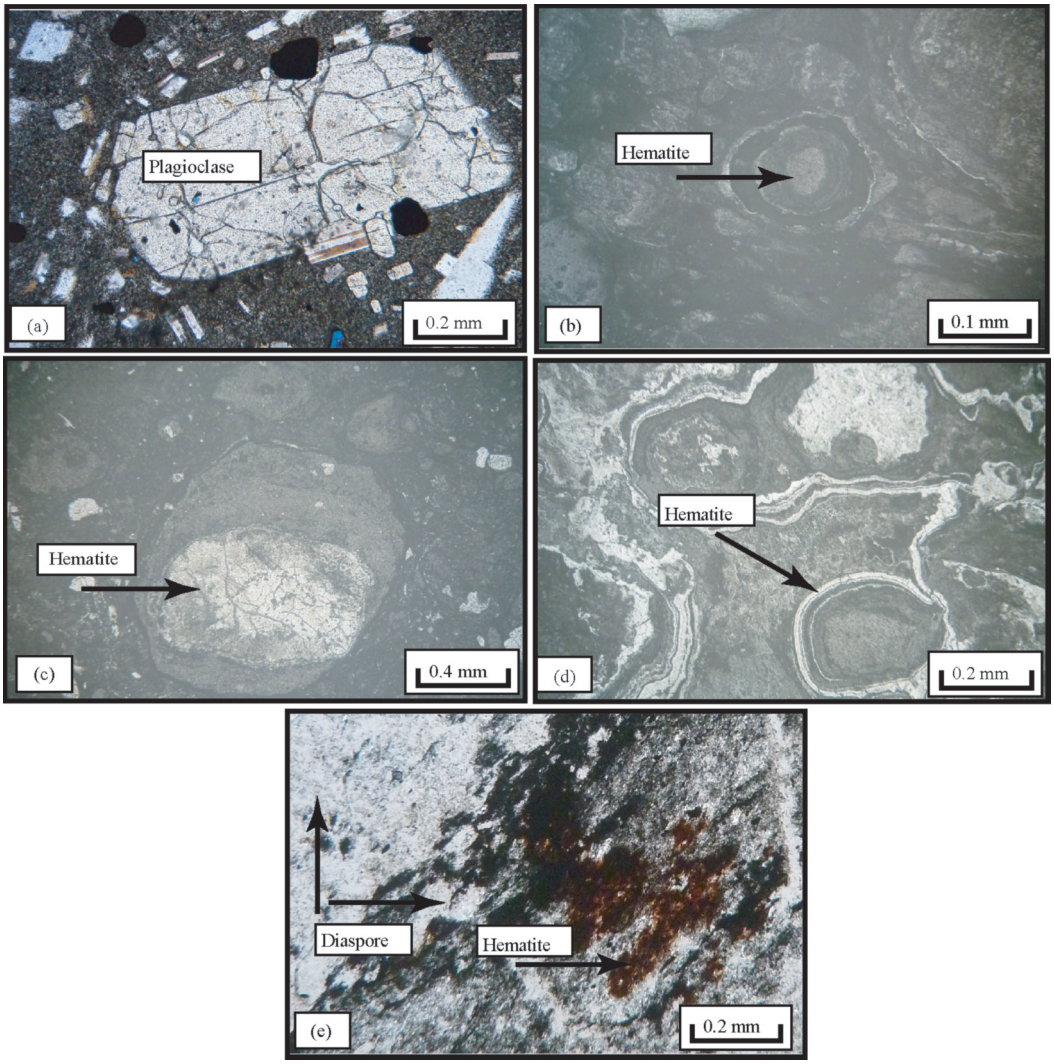

Figure 2. Photomicrographs of basaltic rocks and bauxitic ores. a) Phenocryst of plagioclase in basalt (cross-polarized light). b) Ooids with hematitic nucleus in the bauxitic ores (polarized reflective light). c) A pisoid with hematitic nucleus in the bauxitic ores (polarized reflective light). d) Hematitic concentric bands in the bauxitic ores (polarized reflective light). e) Diaspore along with hematite in the bauxitic ores (cross-polarized light).

Table 1. Results of chemical analyses obtained by ICP-MS method for the studied samples. The detection limits of various elements also are shown in this table. Values of oxides and L.O.I. are in wt% also trace and rare earth elements are in ppm.

	Detection limit	Basalt		Bauxite					
Sample No		S-1	S-2	R-1	R-2	R-3	R-4	R-5	R-6
SiO_2	0.01	51.42	50.92	17.81	16.63	14.34	19.12	11.86	14.84
Al_2O_3	0.01	18.32	18.74	39.12	37.82	39.21	36.41	40.38	40.01
Fe_2O_3	0.01	10.6	10.9	24.99	27.77	29.35	25.84	30.9	27.3
CaO	0.01	6.54	7.14	0.17	0.18	0.17	0.21	0.16	0.09
Na_2O	0.01	5.52	5.23	0.21	0.12	0.11	0.12	0.11	0.1
MgO	0.01	2.35	2.55	0.19	0.17	0.15	0.22	0.12	0.16
K_2O	0.01	1.54	1.34	0.79	0.46	0.27	0.54	0.09	1.74
TiO_2	0.01	2.08	2.09	4.87	4.83	4.91	4.58	5	5.23
MnO	0.01	0.15	0.18	0.04	0.06	0.06	0.07	0.08	0.04
Cr_2O_3	0.001	0.021	0.032	0.061	0.071	0.072	0.061	0.093	0.072
P_2O_5	0.01	0.22	0.19	0.09	0.08	0.08	0.09	0.07	0.08
L.O.I	0.10	0.69	0.54	11.14	11.49	10.72	12.21	10.99	10.02
Sum	-	99.451	99.852	99.481	99.681	99.442	99.471	99.853	99.682
U	0.1	5.5	7.5	10.9	12.2	12.4	11.7	10.6	10.6
Th	0.2	22.5	28.8	25.4	25.3	26.1	24.7	26.9	32.1
Ba	1	347	387	27	24	25	27	21	24
Hf	0.1	13.1	9.7	15.4	14.1	14.8	14.6	15.6	17.7
Co	0.2	97.2	102.3	55.4	56	58.6	59	61.2	43.1
Nb	0.1	22.4	18.7	92.7	91.8	94.1	84.8	96.1	104.2
Cs	0.1	0.2	0.4	1.2	1.3	1.2	1.6	1.1	0.9
Rb	0.1	18.7	31.2	27.8	7.2	5.4	14.7	3.4	56.4
V	8	135	165	751	692	777	698.1	845	765
Ga	0.5	13.2	8.7	29.3	27.5	28.0	27.0	29.1	31.2
Sn	1	2	2	5	4.3	4	4	5	7
Sr	0.5	242.2	251.2	52.1	47.3	41.2	52.7	35.4	48.2
W	0.5	2.2	3.1	5.2	5.1	5.3	5.2	5.1	5.4
Y	0.1	22.8	29.1	62.1	56.2	56.1	58.7	57.8	59.1
Sc	1	13	11	22	25	26	22	27	24
Be	1	2	1	4	5	5	4	5	5
Ta	0.1	8.7	8.5	8.9	8	8.2	7.59	9.8	10.2
Zr	0.1	457.2	354.2	471.8	446.2	449.1	442.8	465.8	460.5
Pb	0.1	9.2	9.4	24.1	22.4	23.6	22.0	24.4	24.1
Ni	0.1	121.1	94.2	274.1	323.2	323.1	278.2	343.2	247.3
La	0.1	16.7	15.8	82.0	101.2	109.6	100.2	131.5	120.3
Ce	0.1	30.6	30.2	199.2	385.4	417.6	218.5	501.1	262.2
Pr	0.02	3.71	3.78	28.0	33.0	35.8	35.0	42.9	42.0
Nd	0.3	17.0	17.3	143.3	174.1	188.6	176.0	226.4	211.2
Sm	0.05	4.41	4.52	34.1	37.9	41.1	40.8	49.3	49.0
Eu	0.02	1.46	1.50	9.11	10.02	10.86	10.45	13.03	12.54
Gd	0.05	4.91	4.92	25.41	23.82	25.71	28.72	30.91	34.51
Tb	0.01	0.74	0.79	3.72	3.82	4.13	4.12	4.96	4.95
Dy	0.05	4.09	4.26	19.37	19.68	21.32	21.19	25.58	25.43
Ho	0.02	0.78	0.79	3.33	3.41	3.69	3.69	4.43	4.43
Er	0.03	1.98	2.05	9.41	9.66	10.47	10.47	12.56	12.56
Tm	0.01	0.24	0.25	1.33	1.33	1.44	1.42	1.73	1.70
Yb	0.05	1.52	1.58	8.42	8.42	9.13	9.13	10.95	10.95
Lu	0.01	0.21	0.23	1.18	1.88	1.27	1.26	1.53	1.51

Table 1. Continued...

	Bauxite								
Sample No	R-7	R-8	R-9	R-10	R-11	R-12	R-13	R-14	R-15
SiO_2	12.53	21.47	29.28	19.46	22.47	16.91	26.62	15.12	30.11
Al_2O_3	43.05	35.23	29.87	39.76	45.55	39.16	30.9	49.65	41.61
Fe_2O_3	26.78	23.69	24.82	21.73	12.41	25.25	22.88	16.79	7.67
CaO	0.09	0.21	0.33	0.09	0.17	0.16	0.29	0.2	0.41
Na_2O	0.12	0.14	0.21	0.12	0.11	0.11	0.12	0.11	0.13
MgO	0.13	0.19	0.31	0.2	0.24	0.18	0.26	0.16	0.29
K_2O	1.12	0.42	3.84	3.02	1.75	0.78	0.42	0.84	2.6
TiO_2	5.19	4.69	2.97	5.47	5.55	4.94	3.65	5.85	5.11
MnO	0.06	0.04	0.04	0.08	0.06	0.06	0.09	0.04	0.06
Cr_2O_3	0.061	0.062	0.061	0.082	0.031	0.062	0.081	0.042	0.021
P_2O_5	0.09	0.1	0.09	0.15	0.16	0.08	0.12	0.13	0.15
L.O.I	10.69	13.54	8.03	9.15	11.12	11.85	14.11	10.87	11.23
Sum	99.911	99.782	99.851	99.312	99.621	99.542	99.541	99.822	99.391
U	12.1	12.8	12.1	15	15.1	10.9	11.5	14.8	15.2
Th	26.8	24.2	21.1	26.8	31.1	25.5	22.6	31	30.9
Ba	28	30	28	45	48	25.1	35.4	40.2	46.5
Hf	16.6	14.5	14.5	16.6	19.1	15.6	14.7	18.7	17.8
Co	57.8	52.9	55.3	52.5	49.4	55.4	68.4	40.3	58.2
Nb	95.9	87.3	64.1	101.3	112.6	92.1	64.01	121.6	98.9
Cs	1.2	1.5	8.2	5.3	1.7	1.2	2.5	0.2	3.1
Rb	42.5	12.7	114.4	82.1	47.5	27.5	17.2	7.9	87.2
V	761	701	655	714	601	729	667	664	521
Ga	29.9	28.2	23.8	28.5	35.4	29.1	24.6	37.0	33.3
Sn	5	4	4	5	6	5	5	6	6
Sr	37.5	42.1	87.6	58.2	52.1	50.9	45.2	42.3	60.2
W	5.2	5.1	5.2	6.3	8.2	5	3	8	6
Y	63.7	53.2	45.1	62.4	64.5	61.1	52.4	65.2	63.6
Sc	23	20	21	18	9	22	19	13	4
Be	4	4	4	4	2	4	5	3	1
Ta	11.4	8.2	7.2	10.1	11.5	9.9	6.9	11.9	11.3
Zr	495.2	422.2	376.3	465.6	501.4	459.2	404.6	523.6	476.7
Pb	26.0	21.0	17.9	23.9	33.5	23.5	18.4	29.6	25.1
Ni	261.2	298.3	216.4	242.4	82.1	281.1	182.2	53.4	109.1
La	98.4	77.1	75.7	77.0	34.1	100.2	83.5	44.3	41.3
Ce	239.0	168.1	183.8	87.0	87.5	113.1	94.3	113.8	130.2
Pr	33.5	26.9	25.8	28.1	12.1	36.5	30.4	15.7	14.2
Nd	171.9	135.4	132.2	144.1	61.5	187.4	156.1	80.0	71.5
Sm	40.9	31.4	31.4	32.6	14.2	42.4	35.4	18.5	16.3
Eu	10.94	8.04	8.41	8.38	3.84	10.89	9.07	4.99	4.15
Gd	30.41	22.12	23.44	22.31	10.72	29.01	24.21	13.92	11.21
Tb	4.46	3.17	3.43	3.10	1.54	4.02	3.35	2.00	1.44
Dy	23.24	16.30	17.88	16.32	8.27	21.22	17.68	10.75	7.55
Ho	3.99	2.84	3.07	2.89	1.34	3.76	3.13	1.74	1.28
Er	11.29	8.05	8.69	8.21	3.79	10.67	8.89	4.93	3.18
Tm	1.59	1.09	1.22	1.09	0.49	1.42	1.18	0.88	0.54
Yb	10.11	7.02	7.78	7.09	3.52	9.22	7.68	4.58	2.51
Lu	1.42	0.97	1.09	1.67	0.45	1.75	1.77	0.59	0.42

Table 1. Continued...

	Bauxite							
Sample No	R-16	R-17	R-18	R-19	R-20	R-21	R-22	R-23
SiO_2	28.33	34.92	21.82	20.91	19.52	25.83	17.12	15.64
Al_2O_3	29.66	30.8	35.1	42.66	41.68	37.71	42.96	40.07
Fe_2O_3	21.1	17.66	24.11	17.07	20.09	18.61	21.65	26.31
CaO	0.42	0.49	0.22	0.13	0.17	0.4	0.16	0.12
Na_2O	0.11	0.12	0.11	0.12	0.11	0.15	0.12	0.11
MgO	0.28	0.29	0.23	0.24	0.21	0.27	0.14	0.11
K_2O	1.24	0.37	0.62	2.37	1.11	2.79	0.92	1.55
TiO_2	2.88	3.08	4.28	5.51	5.19	4.26	5.27	5.23
MnO	0.05	0.11	0.07	0.07	0.06	0.05	0.07	0.08
Cr_2O_3	0.052	0.041	0.063	0.041	0.050	0.051	0.051	0.072
P_2O_5	0.13	0.08	0.09	0.15	0.13	0.12	0.11	0.1
L.O.I	15.45	11.46	12.99	9.63	11.3	9.57	10.55	10.41
Sum	99.722	99.421	99.73	98.911	99.620	99.811	99.121	99.822
U	15.9	12.2	11.2	13.5	13.6	13.5	14.8	13.3
Th	16.1	21	24.1	28.9	28.2	26.1	29	26.8
Ba	41	25.6	28.4	45.1	41.2	38.7	35.2	30.2
Hf	13.5	12.4	15.2	17.85	16.58	16.8	17.35	16.1
Co	55.1	87.3	62.1	50.9	52.7	52.3	55.3	56.8
Nb	52.3	58.2	78.1	106.9	102.3	88.3	104.3	98.8
Cs	3.2	2.3	1.9	3.3	1.2	4.7	1.1	3.2
Rb	41.4	14.9	22.4	64.8	27.3	80.9	25.4	42.7
V	606	640	701	657	646	628	644	700
Ga	23.7	24.2	26.7	31.8	31.4	29.6	32.2	29.0
Sn	3	3	5	5	5	5	5	5
Sr	54.6	50.1	30.2	55.1	49.7	69.8	43.7	46.8
W	3	3	4	7	6	6	6	5
Y	44.2	41.6	58.2	63.45	57.4	56.2	61.15	60.1
Sc	17	17	22	19	18	15	18	23
Be	3	3	5	4	4	3	4	5
Ta	6.1	6.5	8.5	10.8	9.7	9.3	10.6	9.9
Zr	364.1	384.3	432.6	483.2	473.2	438.2	483.1	465.5
Pb	17.0	18.5	20.8	25.4	25.0	22.4	25.8	24.4
Ni	162.5	136.2	232.1	162.2	202.2	149.1	212.2	292.1
La	53.7	49.6	53.7	64.2	40.9	53.2	63.1	84.3
Ce	169.3	156.2	169.3	72.5	105.0	136.5	153.2	321.2
Pr	18.5	17.0	18.5	23.4	14.5	18.9	21.5	27.5
Nd	93.0	85.8	93.0	120.1	73.8	95.9	110.2	145.1
Sm	21.2	19.6	21.2	27.2	17.0	22.2	26.2	31.6
Eu	5.40	4.98	5.40	6.98	4.61	5.99	7.01	8.35
Gd	25.01	23.02	25.01	18.64	12.81	16.72	19.51	19.83
Tb	1.87	1.73	1.87	2.58	1.85	2.40	2.86	3.18
Dy	9.82	9.06	9.82	13.60	9.92	12.90	14.90	16.40
Ho	1.66	1.54	1.66	2.41	1.61	2.09	2.56	2.84
Er	3.81	3.55	3.81	6.84	4.55	5.91	7.24	8.05
Tm	0.54	0.78	0.54	0.91	0.59	0.76	1.02	1.11
Yb	2.48	2.98	2.48	5.91	4.22	5.49	6.48	7.02
Lu	0.45	0.48	0.45	1.98	0.54	0.70	0.91	0.98

opaque minerals. Plagioclase occurs as fine to medium-grained (1-3mm) subhedral to euhedral, occasionally zoned, they displaying Carlsbad and albitic twinning. Some are partially altered to fine-grained aggregates of chlorite, sericite, calcite, and opaque minerals. Ferromagnesian minerals are chiefly augite and olivine were altered to serpentine, chlorite, tremolite, and opaque minerals. The opaques are mainly pyrite (2 -7%) and ilmenite (1-3%).

Petrographic studies of the bauxitic samples are represented that texture-making units include nodes, ooids, pisoids set in a pelitomorphic matrix. Hematite and diaspore are the most important and distinguishable minerals in these samples. Hematite is seen as nodes and nucleus of ooids (Figure 2b) and pisoids (Figure 2c) and occasionally as concentric bands (Figure 2d) and scaly aggregates. Diaspore is seen as tabular and elongate crystals along with hematite set in a pelitomorphic matrix (Figure 2e). Regarding to the mode of distribution of texture-making units and matrix, the ores display pelitomorphic, colloform, fluidal-collomorphic, spongy, nodular, ooidic, and pisoidic textures. The presence of pelitomorphic, fluidal-collomorphic, spongy, nodular, ooidic, and pisoidic textures in the ores indicate an authigenic mode of formation for this deposit (Bardossy, 1982). The pelitomorphic and colloformic textures imply an indirect bauxitization and weak draining processes during the evolution of this deposit. The development of hematitic nodules in the ores can be attributed to factors such as variation in water activity in pedogenic environments (Tardy and Nahon, 1985) and/or climatic fluctuations (Mongelli, 2002).

Analytical mineralogy

XRD analyses illustrated that the bauxitic ores are made of diaspore, hematite, and kaolinite as major mineral phases accompanied by various proportions of boehmite, muscovite- illite, goethite, rutile, and montmorillonite (Table 2). It is worthy to note that rutile, as a major controlling mineral phase for Ti, is restricted to ores which is goethite is more abundant than hematite in them (Table 2).

Table 2. Mineralogical compositions for the bauxitic ores at Kanigorgeh.

Sample No	Mineral composition							
	Montmorillonite	Rutile	Muscovite-Illite	Goethite	Hematite	Kaolinite	Boehmite	Diaspore
R-1	x	x	xx	x	xx	xx	n.d.	xxx
R-3	n.d.	x	x	x	xxx	xx	n.d.	xxx
R-5	n.d.	x	x	x	xxx	xx	n.d.	xxx
R-7	n.d.	xx	xx	xx	xx	xx	xx	xx
R-9	x	x	xxx	x	xxx	x	n.d.	xx
R-11	n.d.	xx	xx	xx	xx	xx	x	xxx
R-13	n.d.	x	x	n.d.	xx	xx	n.d.	xxx
R-15	n.d.	xx	xx	xx	x	xx	xx	xx
R-17	n.d.	x	x	xx	x	xxx	x	xxx
R-19	n.d.	xx	xx	xx	x	xx	x	xxx
R-21	x	x	xx	n.d.	xx	xx	n.d.	xxx
R-23	n.d.	xx	xx	xx	x	xx	x	xxx

Note: The percentage of minerals in given in a symbol form as follows: xxx = > 25%; xx = 5-25%; x = < 5 %; n.d.= not detected.

Geochemistry of bauxitic ores

Geochemistry of major and minor elements. Chemical analyses showed that the principal constituents of the bauxitic ores include SiO_2 (11.86-30.11 wt%), Al_2O_3 (29.66-46.65 wt%), Fe_2O_3 (7.67-30.90 wt%), and TiO_2 (2.88-5.85wt%) (Table1). These values almost display wide range of variations. LOI ranges from 8.03 to 15.45 wt%. Alkali and alkali earth elements along with P, Mn, and Cr (as oxides) are present in rather low concentrations and form 0.72-3.83wt% of the ores in total. Trivariate plot of SiO_2-Al_2O_3-Fe_2O_3 (Boulangé et al., 1996) denotes that despite notable variation in concentration values of Si, Al, and Fe, the residual ores have composition within the range of argillo-ferruginous-bauxite (Figure 3a). Also, plotting the Kanigorgeh data on trivariate diagram SiO_2-Al_2O_3-Fe_2O_3 (Schellmann, 1982) attests to the formation of the above ores under moderate to intense lateritization conditions (Figure 3b).

Geochemistry of trace and rare earth elements. According to the analytical data, the trace elements that are present in relatively notable quantity in the argillo-ferruginous-bauxite ores include V (521-765 ppm), Zr (364.1-523.6 ppm), and Ni (53.4-298.3 ppm). Other trace elements such as Cs, Sn, W, and Be are present in a small amount of ppm; Ta, Sc, and Rb in a few to a few tens of ppm; and Th, U, Cu, Ba, Hf, Co, Nb, Sr, Y, and Pb in a few tens of ppm. REEs are present in the range of 291.90 to 1056.88 ppm (LREEs and HREEs have ranges 223.96 - 995.14 ppm and 16.92 - 61.74 ppm, respectively).

Discussion

Elemental ratios in the ores

In this study, we try to consider pH range of the formation environment and the initial composition of the ores with various elemental ratios. Variation of La/Y is an effective parameter

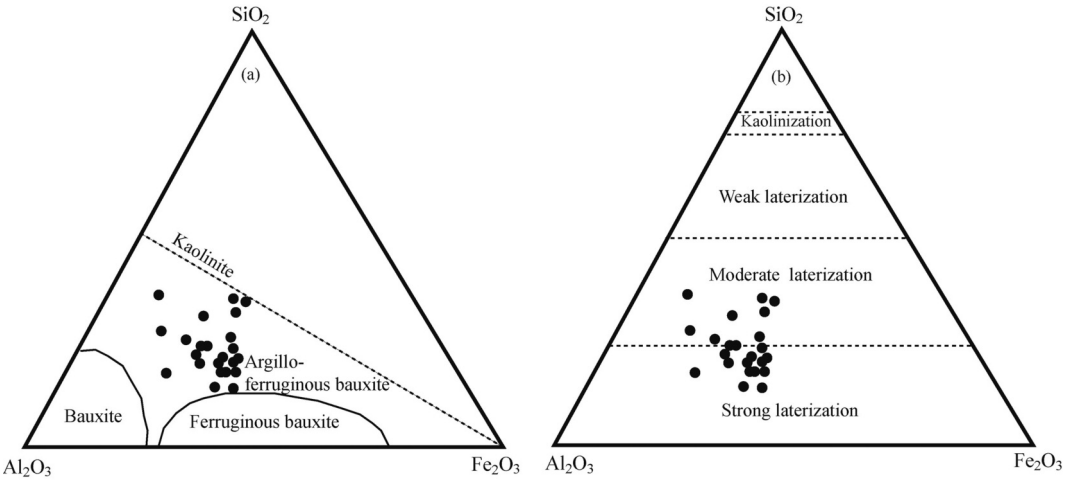

Figure 3. Two trivariate plots of SiO_2 - Al_2O_3 - $Fe_2O_{3\,(T)}$ showing classification of bauxites, a) presented by Boulangé et al. (1996) and b) presented by Schellmann (1982). Filled circles on these plots belong to data of the bauxitic ores at Kanigorgeh.

for determining the pH of the deposition environment of bauxitic ores so that ratios of <1 and > 1 are indicative of acidic and basic environment for bauxite formation, respectively (Crinci and Jurkowic, 1990). The values of La/Y show a range 0.52-2.72 (with an average 1.33). This range points to the fact that increasing pH of weathering solutions was one of effective factors for development of the studied ores.

Considering the concentrations or proportion of selected trace elements, Mordberg (1993) proposed several variation diagrams that can be used to distinguish the mineralogical composition of bauxite deposits of different ages. These diagrams were utilized for determination of the initial composition of bauxitic ores at Kanigorgeh. Mordberg (1993) introduced three bivariate diagrams Pb-Y (Figure 4a), Pb-Ga (Figure 4b), and Zr/Pb-Cr/Ni (Figure 4c) for recognition of mineralogical composition of bauxitic deposits with various ages. Data points of argillo-ferruginous-bauxite at Kanigorgeh in these diagrams hint to an original gibbsitic composition for the ores which were converted to boehmite and diaspore with passing time.

Parental affinity

Most lateritic bauxites can be directly related, through their textures and composition, to the underlying source rocks (Bardossy and Aleva, 1990; Mondillo et al., 2011), but this is rarely seen in the bauxites developed above carbonate sequences. Despite the well-constrained stratigraphic framework for bauxite formation, the origin of the Permian karst bauxites in the Kanigorgeh, as others in northwestern Iran,

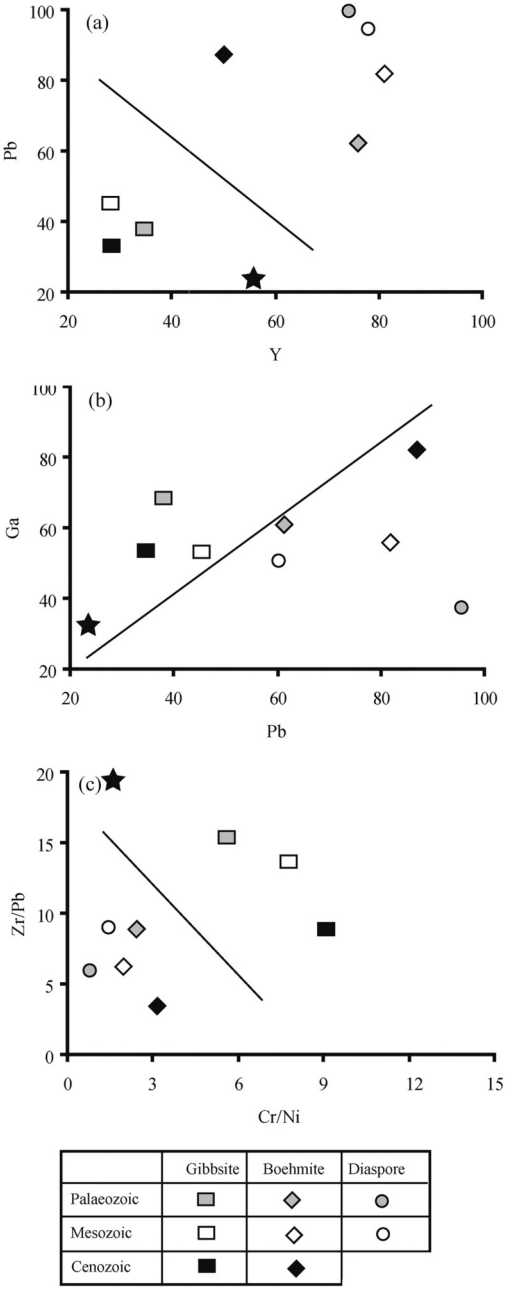

Figure 4. Bivarite plots of a) Pb-Y, b) Ga-Pb, and c) (Zr/Pb)-(Cr/Ni) for various bauxitic minerals (gibbsite, boehmite, and diaspore) of different ages (Paleozoic, Mesozoic, and Cenozoic) (Mordberg, 1993). The data points of bauxitic ores at Kanigorgeh are shown on these plots (in the form of star).

remains controversial. The dissolution of the host carbonate to leave an insoluble residue is not considered a viable mechanism for bauxite formation, because the host carbonates are too pure.

For determination of parent rock(s) of the ores various geochemical diagrams that are designed on the basis of concentration values of elements such as Ni, Cr, Zr, Ga, Mn, Sc, Nb, Y, and Ti, were used.

Concentration values of Cr and Ni in the ores. Illustration of concentration values of Cr and Ni of the ores on bivariate diagrams of Log Cr-Log Ni (Schroll and Sauer, 1968) demonstrate that the bauxitic ores at Kanigorgeh lie on the field of karst bauxite near to the basaltic precursor (Figure 5).

Accumulation coefficients of trace elements. For calculation of accumulation coefficient of trace elements (Ni, Cr, Zr, Ga, Mn, and Sc) the following equation presented by Shaw (1964) was utilized:

$R = \Sigma_n(i=1)\ K_i / K_l$

In this equation, R = accumulation coefficient of the trace element, i = the given trace element, n = the number of trace elements used, K_i = the average concentration values of trace elements in the profile, and K_l = the average concentration values of trace elements in the lithosphere (Mason and Moore, 1982).

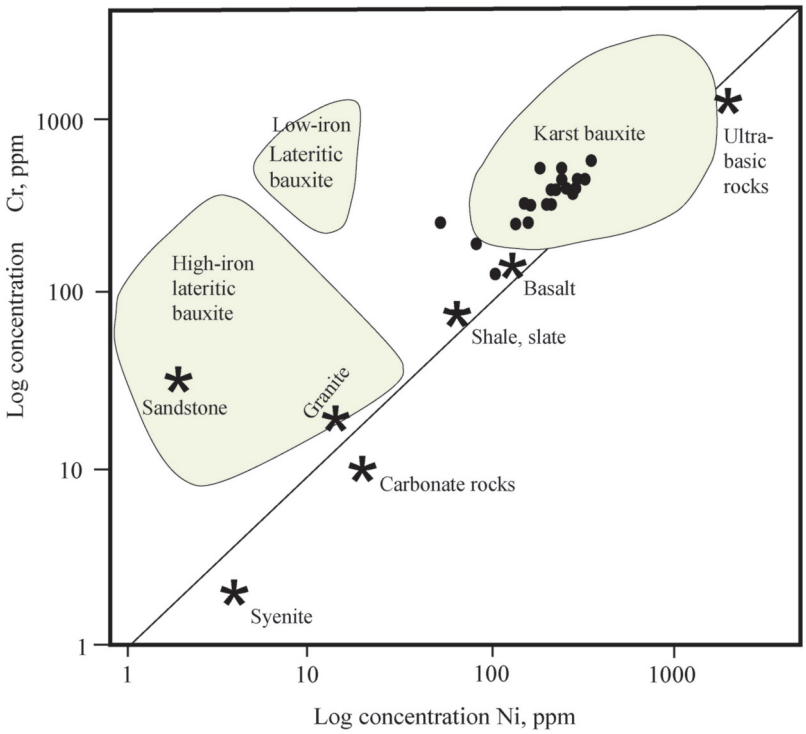

Figure 5. A bivariate plot illustrating the concentration variations of Ni versus Cr in karstic and lateritic bauxites with different parent rocks (after Schroll and Sauer, 1968). Filled circles belong to the data of the bauxitic ores at Kanigorgeh.

Since the values of accumulation coefficient of trace elements (R) cannot determine the lithologic characteristics of the parent rocks by itself (from which the bauxitic deposits were derived), therefore they should be normalized by a more or less genetically stable element like Cr (Özlü, 1983). The bivariate diagram of R-Cr (Özlü, 1983) shows that the data points of Kanigorgeh plot within the field of laterites derived from basalts (the field of mafic igneous parent rocks) (Figure 6).

Values of Zr/TiO_2 and Nb/Y of the ores. Floyd and Winchester (1978) utilized Zr/TiO_2 and Nb/Y for determination of parent rock(s) composition of the laterites especially when the parent rock(s) is a volcanic igneous rock. The calculated correlation coefficients among Zr, Ti, Nb, and Y in Kanigorgeh bauxites have a range between 0.89 to 0.97 (Table 3). The values show that (1) these elements have very analogous geochemical behavior during bauxitization processes and (2) these ratios remained constant during bauxitization, so they can be used for determination of the parent rocks. The data points of the ores on the bivariate diagram of Zr/TiO_2 - Nb/Y (Floyd and Winchester, 1978) indicates a basaltic parent rock (Figure 7).

Calculation of mass changes during bauxitization. Many weathering indexes including chemical index of alteration (CIA) and chemical index of weathering (CIW) were proposed to assess the intensity of weathering

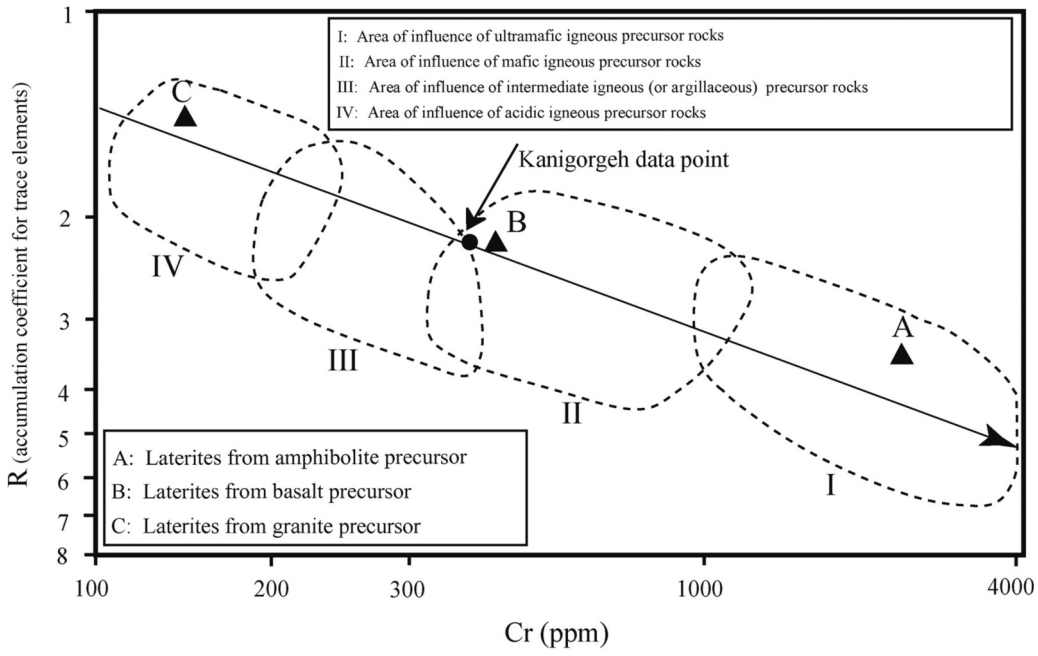

Figure 6. Log Cr vs. accumulation coefficient values, R (for calculation of R see text) with indication of the influence area of various precursor rocks (e.g., amphibolite, basalt and granite) (after Özlü, 1983). A, B and C represent laterites from amphibolite, basalt, and granite precursors, respectively. The numbers I, II, III and IV represent the area of influence of ultramafic, mafic, intermediate (or argillaceous), and acidic precursor rocks, respectively. The Kanigorgeh data plots adjacent to B (basalt) within the domain of mafic precursor rocks.

Table 3. Spearman correlation coefficient values among elements in the bauxitic ores at Kanigorgeh.

	Si	Al	Fe	Ca	Na	Mg	K	Ti	Mn	Cr	P	U	Th	Ba	Hf	Co	Nb	Cs	Rb	V	Ga	Sn	Sr	W
Si	1.00																							
Al	-0.62	1.00																						
Fe	-0.59	-0.24	1.00																					
Ca	0.88	-0.59	-0.46	1.00																				
Na	0.29	-0.30	0.02	0.24	1.00																			
Mg	0.93	-0.56	-0.59	0.79	0.35	1.00																		
K	0.35	0.01	-0.41	0.13	0.39	0.45	1.00																	
Ti	-0.71	0.93	-0.09	-0.76	-0.34	-0.65	-0.03	1.00																
Mn	0.22	-0.21	-0.03	0.14	-0.39	0.05	-0.25	-0.16	1.00															
Cr	-0.48	-0.27	0.87	-0.44	-0.03	-0.49	-0.27	-0.06	0.16	1.00														
P	0.32	0.33	-0.80	0.10	-0.11	0.39	0.50	0.26	-0.03	-0.55	1.00													
U	0.29	0.28	-0.69	0.22	-0.17	0.24	0.39	0.15	-0.07	-0.57	0.82	1.00												
Th	-0.49	0.88	-0.27	-0.54	-0.27	-0.43	0.14	0.89	-0.18	-0.23	0.29	0.12	1.00											
Ba	0.34	0.32	-0.82	0.15	-0.11	0.41	0.51	0.23	-0.04	-0.59	0.99	0.84	0.27	1.00										
Hf	-0.34	0.85	-0.46	-0.44	-0.20	-0.23	0.38	0.78	-0.29	-0.37	0.58	0.38	0.88	0.57	1.00									
Co	0.49	-0.60	0.05	0.51	0.01	0.30	-0.34	-0.59	0.77	0.08	-0.34	-0.29	-0.54	-0.33	-0.69	1.00								
Nb	-0.66	0.96	-0.17	-0.68	-0.26	-0.58	0.08	0.97	-0.26	-0.16	0.30	0.21	0.93	0.28	0.85	-0.67	1.00							
Cs	0.55	-0.46	-0.16	0.37	0.51	0.59	0.82	-0.47	0.00	0.00	0.25	0.22	-0.36	0.26	-0.15	0.07	-0.40	1.00						
Rb	0.40	-0.08	-0.39	0.19	0.42	0.50	0.98	-0.11	-0.23	-0.27	0.44	0.32	0.08	0.45	0.31	-0.25	-0.03	0.82	1.00					
V	-0.74	0.07	0.87	-0.62	-0.06	-0.70	-0.43	0.22	0.00	0.80	-0.69	-0.71	0.03	-0.73	-0.18	-0.03	0.13	-0.33	-0.42	1.00				
Ga	-0.41	0.95	-0.46	-0.41	-0.25	-0.35	0.11	0.85	-0.30	-0.46	0.46	0.37	0.90	0.46	0.92	-0.63	0.92	-0.41	0.02	-0.15	1.00			
Sn	-0.39	0.70	-0.24	-0.47	-0.19	-0.30	0.23	0.70	-0.28	-0.11	0.29	0.00	0.87	0.26	0.86	-0.59	0.74	-0.25	0.21	0.03	0.76	1.00		
Sr	0.55	-0.30	-0.31	0.42	0.61	0.64	0.82	-0.37	-0.26	-0.26	0.28	0.24	-0.18	0.29	-0.01	-0.12	-0.24	0.82	0.80	-0.47	-0.18	-0.12	1.00	
W	-0.36	0.85	-0.40	-0.44	-0.03	-0.22	0.37	0.78	-0.38	-0.38	0.51	0.41	0.79	0.50	0.85	-0.71	0.87	-0.07	0.24	-0.14	0.87	0.60	0.13	1.00
Y	-0.63	0.88	-0.15	-0.68	-0.21	-0.52	0.06	0.93	-0.19	-0.12	0.32	0.11	0.83	0.29	0.81	-0.57	0.89	-0.39	0.00	0.14	0.81	0.75	-0.30	0.73
Sc	-0.57	-0.24	0.97	-0.47	0.00	-0.55	-0.41	-0.07	0.05	0.82	-0.79	-0.73	-0.26	-0.81	-0.46	0.11	-0.16	-0.17	-0.40	0.86	-0.46	-0.27	-0.33	-0.39
Be	-0.55	-0.20	0.88	-0.54	-0.10	-0.54	-0.38	0.00	0.13	0.86	-0.62	-0.66	-0.15	-0.66	-0.33	0.05	-0.08	-0.16	-0.39	0.77	-0.39	-0.10	-0.39	-0.35
Ta	-0.49	0.93	-0.33	-0.53	-0.24	-0.44	0.24	0.87	-0.20	-0.30	0.39	0.28	0.89	0.39	0.92	-0.58	0.90	-0.27	0.18	0.00	0.92	0.79	-0.17	0.81
Zr	-0.65	0.98	-0.19	-0.65	-0.26	-0.58	-0.02	0.95	-0.16	-0.19	0.29	0.17	0.89	0.27	0.83	-0.54	0.95	-0.48	-0.10	0.14	0.91	0.73	-0.34	0.80
Pb	-0.51	0.94	-0.32	-0.54	-0.27	-0.44	0.04	0.86	-0.18	-0.33	0.39	0.30	0.85	0.37	0.85	-0.54	0.91	-0.42	-0.04	-0.01	0.93	0.69	-0.23	0.87
Ni	-0.56	-0.19	0.88	-0.48	0.05	-0.58	-0.36	0.05	0.02	0.78	-0.71	-0.62	-0.18	-0.74	-0.44	0.09	-0.07	-0.15	-0.32	0.78	-0.40	-0.24	-0.30	-0.33
La	-0.61	-0.09	0.85	-0.48	-0.06	-0.58	-0.31	0.09	0.01	0.79	-0.71	-0.70	-0.02	-0.76	-0.26	0.00	0.00	-0.20	-0.27	0.85	-0.27	0.00	-0.25	-0.25
Ce	-0.51	-0.03	0.71	-0.23	-0.10	-0.57	-0.40	0.04	0.04	0.58	-0.68	-0.44	-0.04	-0.70	-0.31	0.11	0.00	-0.24	-0.38	0.66	-0.20	-0.14	-0.34	-0.21
Pr	-0.59	-0.10	0.83	-0.49	-0.06	-0.55	-0.29	0.09	0.00	0.79	-0.68	-0.71	-0.01	-0.73	-0.24	-0.02	0.00	-0.19	-0.24	0.84	-0.27	0.03	-0.23	-0.25
Nd	-0.60	-0.09	0.84	-0.50	-0.07	-0.56	-0.29	0.10	0.02	0.80	-0.68	-0.70	-0.01	-0.73	-0.24	-0.01	0.01	-0.19	-0.25	0.84	-0.27	0.02	-0.24	-0.24
Sm	-0.59	-0.09	0.84	-0.50	-0.02	-0.55	-0.27	0.09	-0.02	0.78	-0.68	-0.71	-0.01	-0.73	-0.23	-0.03	0.01	-0.18	-0.22	0.84	-0.27	0.03	-0.21	-0.24
Eu	-0.62	-0.07	0.85	-0.51	0.00	-0.57	-0.27	0.11	-0.04	0.79	-0.69	-0.71	0.00	-0.73	-0.22	-0.04	0.02	-0.18	-0.22	0.85	-0.25	0.04	-0.21	-0.22
Gd	-0.36	-0.37	0.82	-0.26	-0.02	-0.34	-0.34	-0.24	0.04	0.70	-0.77	-0.74	-0.33	-0.79	-0.47	0.19	-0.33	-0.15	-0.25	0.77	-0.52	-0.19	-0.26	-0.55
Tb	-0.64	-0.02	0.84	-0.54	0.06	-0.59	-0.24	0.14	-0.11	0.76	-0.68	-0.70	0.04	-0.73	-0.17	-0.09	0.07	-0.18	-0.20	0.84	-0.20	0.07	-0.18	-0.16
Dy	-0.64	-0.02	0.84	-0.54	0.06	-0.59	-0.23	0.14	-0.11	0.76	-0.68	-0.70	0.04	-0.72	-0.16	-0.10	0.07	-0.18	-0.19	0.85	-0.20	0.07	-0.17	-0.15
Ho	-0.63	-0.03	0.83	-0.54	0.05	-0.58	-0.23	0.14	-0.09	0.76	-0.67	-0.70	0.03	-0.71	-0.17	-0.08	0.06	-0.17	-0.19	0.84	-0.21	0.07	-0.17	-0.16
Er	-0.65	0.02	0.81	-0.58	0.06	-0.59	-0.20	0.19	-0.11	0.75	-0.63	-0.67	0.08	-0.68	-0.12	-0.13	0.12	-0.16	-0.18	0.83	-0.16	0.10	-0.15	-0.10
Tm	-0.63	0.02	0.80	-0.51	0.08	-0.60	-0.26	0.16	-0.07	0.71	-0.69	-0.69	0.07	-0.73	-0.16	-0.05	0.10	-0.20	-0.23	0.83	-0.16	0.07	-0.18	-0.13
Yb	-0.66	0.07	0.78	-0.59	0.10	-0.60	-0.18	0.22	-0.13	0.72	-0.60	-0.65	0.13	-0.65	-0.07	-0.15	0.17	-0.16	-0.16	0.81	-0.10	0.13	-0.12	-0.03
Lu	-0.46	0.00	0.55	-0.54	-0.01	-0.36	-0.05	0.21	0.11	0.63	-0.28	-0.48	0.06	-0.34	-0.07	-0.08	0.11	-0.01	-0.06	0.57	-0.16	0.07	-0.06	-0.04

Table 3. Continued...

	Y	Sc	Be	Ta	Zr	Pb	Ni	La	Ce	Pr	Nd	Sm	Eu	Gd	Tb	Dy	Ho	Er	Tm	Yb	Lu
Si																					
Al																					
Fe																					
Ca																					
Na																					
Mg																					
K																					
Ti																					
Mn																					
Cr																					
P																					
U																					
Th																					
Ba																					
Hf																					
Co																					
Nb																					
Cs																					
Rb																					
V																					
Ga																					
Sn																					
Sr																					
W																					
Y	1.00																				
Sc	-0.16	1.00																			
Be	-0.08	0.92	1.00																		
Ta	0.88	-0.33	-0.28	1.00																	
Zr	0.94	-0.18	-0.13	0.93	1.00																
Pb	0.83	-0.33	-0.29	0.89	0.92	1.00															
Ni	-0.03	0.86	0.76	-0.25	-0.11	-0.26	1.00														
La	0.04	0.82	0.71	-0.13	-0.02	-0.17	0.83	1.00													
Ce	-0.09	0.67	0.54	-0.15	-0.03	-0.08	0.71	0.73	1.00												
Pr	0.05	0.80	0.70	-0.12	-0.02	-0.17	0.80	0.99	0.65	1.00											
Nd	0.06	0.81	0.71	-0.11	-0.01	-0.16	0.81	1.00	0.67	0.99	1.00										
Sm	0.06	0.80	0.69	-0.11	-0.01	-0.17	0.80	0.99	0.63	0.99	0.99	1.00									
Eu	0.07	0.81	0.70	-0.09	0.01	-0.14	0.81	0.99	0.65	0.99	0.99	0.99	1.00								
Gd	-0.22	0.80	0.65	-0.36	-0.30	-0.43	0.69	0.84	0.51	0.85	0.84	0.86	0.85	1.00							
Tb	0.10	0.80	0.68	-0.05	0.05	-0.09	0.79	0.97	0.64	0.97	0.97	0.98	0.99	0.82	1.00	1.00					
Dy	0.11	0.79	0.68	-0.04	0.06	-0.09	0.78	0.97	0.63	0.97	0.97	0.98	0.99	0.82	0.99	0.99	1.00				
Ho	0.11	0.79	0.68	-0.05	0.05	-0.10	0.79	0.97	0.61	0.98	0.98	0.99	0.99	0.82	0.99	0.99	0.99				
Er	0.15	0.77	0.67	0.00	0.10	-0.05	0.77	0.96	0.59	0.97	0.97	0.98	0.98	0.78	0.99	0.99	0.99	1.00			
Tm	0.11	0.76	0.63	-0.01	0.09	-0.06	0.73	0.95	0.62	0.95	0.95	0.97	0.97	0.79	0.98	0.98	0.98	0.98	1.00		
Yb	0.18	0.74	0.64	0.04	0.15	0.00	0.74	0.93	0.57	0.94	0.94	0.95	0.96	0.72	0.98	0.99	0.98	0.99	0.98	1.00	
Lu	0.20	0.60	0.60	0.01	0.09	-0.08	0.56	0.74	0.27	0.78	0.78	0.78	0.77	0.55	0.75	0.75	0.77	0.79	0.74	0.78	1.00

processes by Nesbitt and Young (1982) and Harnois (1988). Since these indices are calculated on the basis of concentration values of mobile elements such as Ca, Na, and K, therefore, they have high efficiency for determining of weak to moderate, but not suitable for strong chemical weathering (Nesbitt and Wilson, 1992). Concentration values of CaO, Na_2O, MgO, and K_2O in the weathered products are considerably low compared to basaltic parent rocks (Table 1). These values are comparable to those of reported from intensely weathered zones by Nesbitt and Wilson (1992). Therefore, the intensity of weathering processes in basaltic rocks and hence the evolution of the bauxitic ores can be categorized as extreme (Nesbitt and Wilson, 1992).

Calculation of mass balance is one of proper methods for consideration of mobility and distribution of elements during bauxitization processes. So far, various methods for consideration of behavior of elements during alteration and weathering processes were presented by many researchers. Among these methods, methods of volume factor (Gresens, 1967), isocon (Grant, 1986), and immobile element (MacLean and Kranidiotis, 1987) are the most important ones. In this study because of the authigenic nature of the ores and the basaltic precursor, isocon method (Grant, 1986) was used for estimation of the mobility degree and enrichment of elements, the degree of total mass and volume changes of the system during bauxitization processes. These calculations were implemented systematically based on (1) illustration of bivariate plots, (2) determination of isocon line and its slope, (3) calculation of total mass changes, (4) calculation of volume changes and (5) quantitative determination of the mobility degree and enrichment of elements.

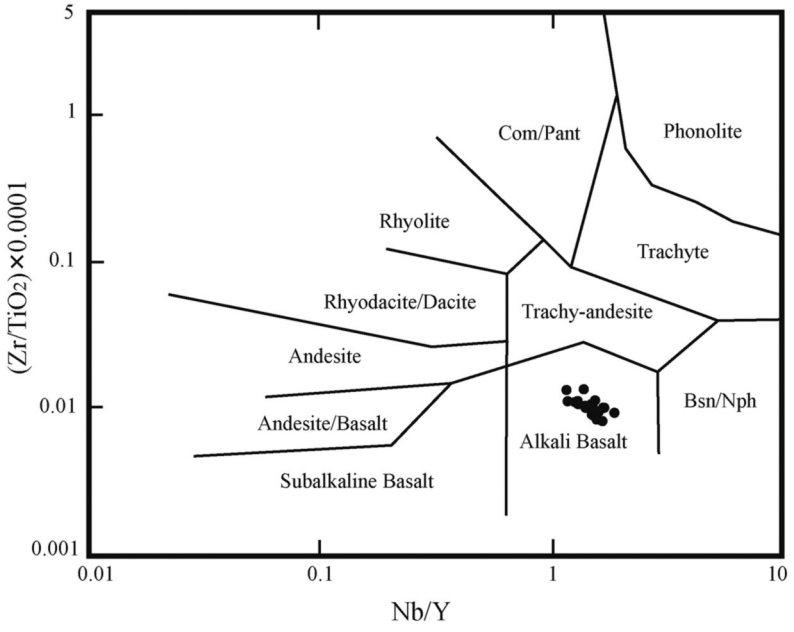

Figure 7. A diagram showing potential parent rock for the bauxitic ores at Kanigorgeh on the basis of Zr/TiO_2-Nb/Y ratios (after Floyd and Winchester, 1978).

Delineation of bivariate plot. By following the Baumgartner and Olsen (1995) diagram, the mean chemical composition of basaltic precursor and bauxitic ores are plotted on abscissa (X axis) and ordinate (Y axis), respectively (Figure 8).

Determination of isocon line and its slope. This method is tried to determine the mobility degree of elements by using immobile elements and delineating isocon line (Grant, 1986). Elements lying on isocon line are considered to be immobile and those lying above and below of this line are enriched and depleted, respectively. In this study, elements such as Zr, Ta, and Th were used for delineating the isocon line (Figure 8). The slope of isocon line is defined by the ratio of the original mass of rock to the mass of altered (weathered) rocks ($S=M^{original}/M^{weathered}$) (Grant, 1986). According to delineated isocon line (Figure 8), the isocon gradient (S) is estimated to be about 1.11.

Calculation of total mass change. For calculation of total mass change in the weathered system during bauxitization of basaltic rocks, the following equation was used:

$\Delta M = [(1/S)-1]*100$ (Grant, 1986)

Where S is the isocon gradient and ΔM is the total mass change.

Based upon this equation, bauxitization of the basaltic rocks was accompanied by a mass decrease of about 9.90%.

Calculation of volume change of the system. With assuming an average density for the basalts (2.67 g/cm^3) and for the bauxitic ores (2.53 g/cm^3), the volume changes were calculated by using the following equation:

$\Delta V = [(1/S)\times(\rho^a/\rho^o)-1]*100$ (Grant, 1986)

Where ΔV is the volume change in percent and ρ^a/ρ^o is the ratio of average density of 23 bauxitic specimens to the studied two basaltic samples.

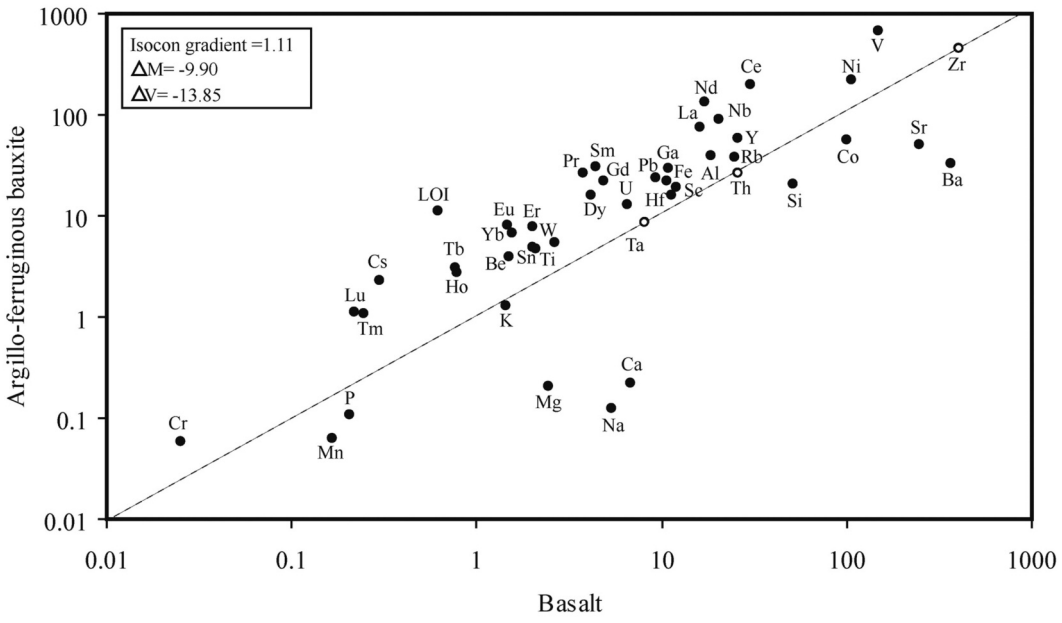

Figure 8. A diagram of isocon mass balance (Grant, 1986) comparing average compositions of argillo-ferruginous- bauxite with the average composition of the basalt. Δ*M* and Δ*V* denote mass and volume changes, respectively.

On the basis of this equation the bauxitization processes of basaltic rocks was accompanied by volume decrease of about 13.85%.

Quantitative determination of the degree of mobility and enrichment of elements. Qualitatively, elements lying above and below the isocon line are meant to be enriched and depleted, respectively during weathering. The absolute compositional change (ΔC) of the constituents is defined as the ratio of concentration change of each element/oxide (C_i^a) to its corresponding original value (C_i^o). ΔC was computed by the following equation:

$\Delta C = (1/S) \times (C_i^a/C_i^o) - 1$ (Grant, 1986)

In order to have better show for elemental variations, the ΔC was multiplied by 100 (% change) and the obtained values are plotted graphically for major, minor, trace, and rare earth elements (see Figure 9a-c). With respect to the delineated graphs in Figure 9, it can become evident that the conversion of basaltic rocks into argillo-ferruginous-bauxite was accompanied by leaching of Si, Ca, K, Na, Mg, Mn, P, Co, Sr, and Ba and enrichment of Al, Fe, Ti, Cr, U, Hf, Nb, Cs, Rb, V, Ga, Sn, W, Y, Sc, Be, Pb, Ni, and REEs.

Controlling factors on mobility, distribution, and enrichment of elements during auxitization

To consider the controlling factors on elements distribution, in addition to the results of mass change computation, it has been tried to calculate the Spearman correlation coefficients among elements (Table 3). This investigation was implemented in two parts (1) leached and (2) enriched elements.

Leached elements

Leached major elements. Regarding the mineralogy of the basaltic parent rock and the bauxitic ores, the depletion of Si from the weathered system can be attributed to the alteration of feldspars and muscovite- illite to kaolinite.

Leached minor elements. The depletion of Na, Ca, and K during bauxitization is due to the breakdown of feldspars in the water-rock reaction systems. Among these elements, K (because of having greater ionic radius) relative to Na suffered lesser depletion. The theory of cation exchange capacity (Wilson, 1994) implies that bigger cations preferably remain on the clay minerals. Distribution of K was controlled by muscovite-illite. The partial depletion of Mg and Mn during the evolution of the ores indicates the decomposition of ferromagnesian minerals and releasing these elements into the weathering solutions. The positive correlation between Si-Ca (r = 0.88) and Si-Mg (r = 0.93) makes clear that the kaolinite acted as fixing agent for Ca and Mg in the ores. Kaolinite, due to having high capacity for cation exchange, can fix large ions like Ca and Mg in the weathered system (Boski and Herbosch, 1990; Mutakyahwa et al., 2003). Depletion of P is likely relates to disintegration of apatite during bauxitization processes.

Leached trace elements. Depletion of Ba from the system may imply that this element had a behavior analogous to alkali and alkali earth elements. Ba normally exhibits quite variable behavior during weathering (Gouveia et al., 1993). It seems that depletion of Ba is owing to breakdown of feldspars during water-rock reaction systems and the partial release of this element into weathering solutions. The positive correlation (r = 0.99) between Ba and P can be the result of controlling role of Al-bearing phosphate minerals such as goreixite [$BaAl_3(PO_4)_2(OH)_5.H_2O$] in distribution of Ba in the ores (Angelica and Da Costa, 1993; Costa and Araujo, 1996). Depletion of Sr shows that as the same with to Ba it is also partially exited from the system. The positive correlation between K and Sr (r = 0.82) illustrates that the distribution of Sr in the ores was controlled by muscovite- illite. Depletion of Co is a result of breakdown of ferromagnesian minerals. The positive correlation

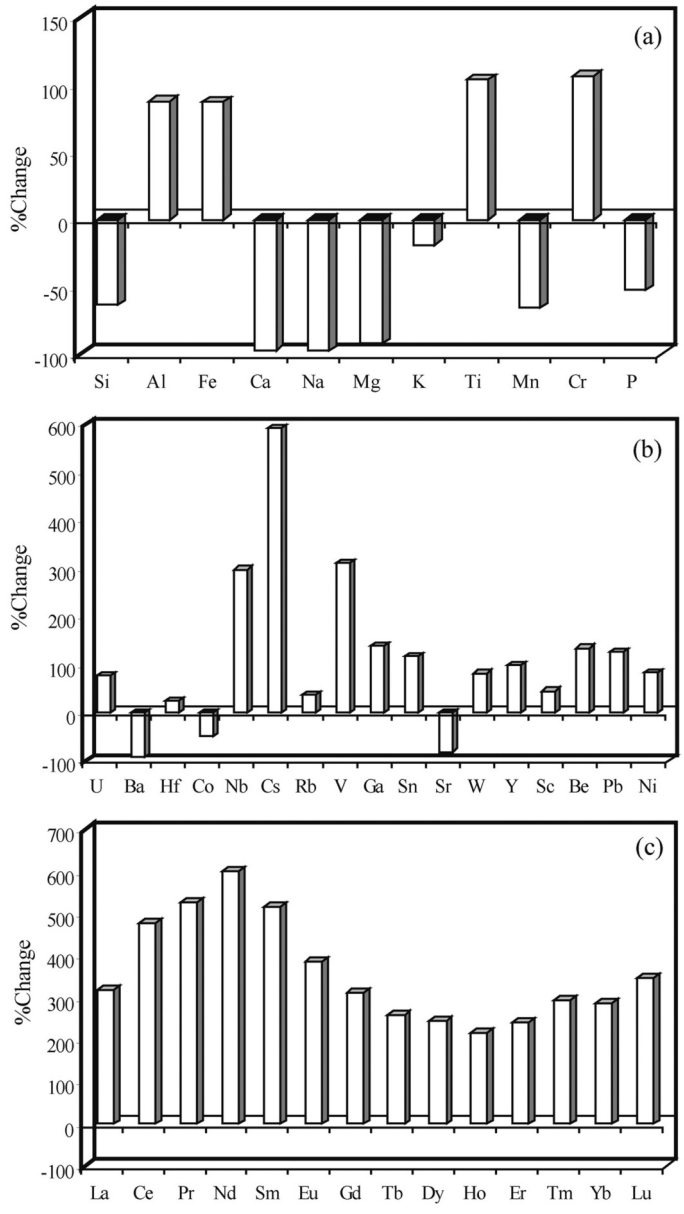

Figure 9. Diagrams illustrating the percentage of elemental mass gains and losses of mean argillo-ferruginous bauxite composition relative to the average basalt composition. a) Major and minor elements. b) Trace elements. c) Rare earth elements.

between Mn and Co (r = 0.77) may imply that the distribution of Co was controlled by Mn-oxides that their presence in the ores are sensitive to the variation of redox conditions (Ma et al., 2007).

Enriched elements

Enriched major elements. Due to lack of variable valence aluminum can be hardly transported by aqueous solutions and commonly act as an immobile element during weathering processes (Nesbitt and Wilson, 1992). So, enrichment of Al during evolution of the ores can be related to its residual concentration as a result of volume reduction in system. It appears that Ti was also enriched analogous to Al. By considering the mineralogy of the parent rocks, it can be inferred that the breakdown of ilmenite and augite provided Ti of the residual system. Augite has typically 0.5 -0.8 wt% TiO_2 (Deer et al., 1992). The enrichment of Fe indicates the prevalence of alkaline pH in the environment of the ore deposition. It appears that buffering of meteoric percolating weathering solutions by carbonate bedrocks facilitated with the fluctuation of underground water table, had an effective role in fixation and enrichment of Fe in the ores. The presence of hematitic nodules in the ores provides a firm reason for fluctuation of the underground water table during development of the ores (Valeton, 1972). The origin of Fe can be related to the oxidation of pyrites and breakdown of ilmenite and ferromagnesian minerals during bauxitization processes.

Enriched trace elements. The positive correlation between pairs of K-Rb (r = 0.98) and K-Cs (r = 0.82) is indicative of the crucial role of muscovite-illite in fixation and concentration of Rb and Cs in the ores. It seems cation exchange processes was notable in enrichment of these two elements relative to other alkali and alkali earth elements. The moderate to good positive correlation between pairs of Ti-W (r = 0.70), Ti-Sn (r = 0.70), and Ti-Ta (r = 0.87) unravels that Ti-bearing mineral phases like rutile played a crucial role in distribution and fixation of W, Sn, and Ta in the ores (Meinhold, 2010).

Vanadium and Cr are often found as co-associated with Fe in natural lateritic Fe-oxide crusts (Marques et al., 2004). Schwertmann and Pfab (1994) proved that V (as V^{3+}) is incorporated with goethite and hematite under surficial weathering conditions. Although Ni can vigorously absorbed by Fe-oxides, the intensity of absorption depends on pH (weaker in lower pH conditions) (Sparks, 1995). The positive correlation between pairs of Fe-V (r = 0.87), Fe-Cr (r = 0.87), and Fe-Ni (r = 0.88) reveals that these three elements were incorporated in the Fe oxy-hydroxides by various mechanisms such as isomorphic replacement, absorption, and/or co-precipitation (Fernández-Caliani and Cantano, 2010) and pH was the most important controlling factor in distribution of these elements in the ores. The positive correlation between Fe-Sc (r = 0.97) suggests that Sc was enriched by similar mechanism to Cr, V, and Ni in the ores (Fernández-Caliani and Cantano, 2010).

The positive correlation between Fe and Be (r = 0.88) shows that Fe-bearing mineral phases like hematite and goethite played an important role in distribution and fixation of Be, and also reveals that pH was the important controlling geochemical factor in distribution of Be in the ores. This deduction also corresponds with Feng (2011).

The positive correlations between pairs of Al-Y (r = 0.88), Al-Th (r = 0.88), and Al-Pb (r = 0.94) indicate that these three elements substituted for Al in diaspore and/ or were adsorbed on the surface of this mineral. Similar results were also reported by Mordberg (1999) for Timan bauxite deposit.

Also, the positive correlation between Al and Zr (r = 0.98) may provide reason for the presence of heavy mineral such as zircon and/ or Zr in diaspore (as isomorphic admixture or absorbed) (Mordberg, 1999). Furthermore, the positive

correlation between pairs of Al-Ga (r = 0.95), Al-Hf (r = 0.85), and Al-Nb (r = 0.96) implies the controlling role of diaspore and clays on distribution and fixation of Ga, Hf, and Nb. Finally, the positive correlation between P and U (r = 0.82) confirms the active role of P-bearing mineral phases (isomorphic with P) in concentration and enrichment of U.

Enriched rare earth elements. Acidity (pH) is the dominant controlling parameter for mobility of REEs during bauxitization (Muzaffer-Karadağ et al., 2009). REEs are leached from weathered products in acidic conditions but are fixed by scavengers in alkaline conditions (Fleet, 1984). Enrichment of REEs is indicative of prevalence of alkaline conditions during evolution of the ores. The evolving secondary minerals also played important role in distribution of REEs during weathering processes (Tripathi and Rajamani, 2007). A few groups of minerals including clays, secondary phosphates, diaspore (due to diadochic substitution) and scavengers like oxides and hydroxides of Fe and Mn were proposed as hosts for REEs in the weathered products by Ma et al. (2007) and Wang et al. (2010). With respect to the correlation coefficients between REEs and Al, Si, Fe, Mn, and P, it could be shown that there is a moderate to good positive correlation between REEs and Fe (r = 0.55 to 0.85). Based on these geochemical correlations, it can be inferred that increasing of pH in weathering solutions by carbonate bedrocks furnished a suitable conditions for absorption of REEs by scavengers like hematite and goethite.

Conclusions

The most important results obtained from geochemical considerations of the argillo-ferruginous-bauxite ores at Kanigorgeh are as follows:

1. According to geochemical data (Ni and Cr values, accumulation coefficients of trace elements, and ratios of immobile elements) basaltic rocks which their remnants are still present in the contact of bauxitic horizon with carbonate bedrocks are the most likely parent rocks for the ores.

2. Ratios of trace elements like Pb/Y, Ga/Pb, Zr/Pb, and Cr/Ni indicate that the ore minerals were initially gibbsitic.

3. Mass balance calculations showed that bauxitization processes of basaltic rocks (as precursor) were accompanied by a decrease of total mass and volume about 9.90% and 13.85%, respectively.

4. Geochemical data revealed that factors such as variation in chemistry of the ore-forming solutions, intensity of lateritization processes, buffering of weathered solutions by carbonate bedrocks, fluctuation of underground water table, cation exchange, isomorphic substitutions, co-precipitation, residual concentration, adsorption, and scavenging by Fe and Mn oxides and hydroxides played substantial role in distribution of elements in the ores at Kanigorgeh.

Acknowledgements

This work was enjoyed financial support by the Research Deputy Bureau of Urmia University. The authors would like to express their thanks and appreciations to the authorities of this bureau, and in particular Prof. Riccardo Petrini, Pisa University, for his precious editorial assistance during the peer review process. Our gratitude is further expressed to three anonymous reviewers for their critical comments on this paper.

References

Angelica R.S. and Da Costa M.L. (1993) - Geochemistry of rare-earth elements in surface lateritic rocks and soils from the Maicuru complex, Para, Brazil. *Journal of Geochemical Exploration,*

47, 165-182.

Bardossy G. (1982) - Karst Bauxites. Elsevier Scientific, Amsterdam, 441 p.

Bardossy, G.Y. and Aleva G.Y.Y. (1990) - Lateritic Bauxites. Akademia, Kiado Budapest, 646 p.

Baumgartner L.P. and Olsen S.N. (1995) - A least square approach to mass transport calculations using the isocon method. *Economic Geology,* 90, 1261-1270.

Boski T. and Herbosch A. (1990) - Trace elements and their relation to the mineral phases in lateritic bauxites from SE Guinea Bissau. *Chemical Geology,* 82, 279-297.

Boulangé B., Bouzat G. and Pouliquen M. (1996) - Mineralogical and geochemical characteristics of two bauxitic profiles, Fria, Guinea Republic. *Mineralium Deposita*, 31, 432-438.

Calagari A.A., Kangrani F. and Abedini A. (2010) - Geochemistry of minor, trace and rare earth elements in Biglar Permo-Triassic bauxite deposit, Northwest of Abgarm, Ghazvin Province, Iran. *Journal of Sciences, Islamic Republic of Iran*, 21, 225-236.

Calagari A.A. and Abedini A. (2007) - Geochemical investigations on Permo-Triassic bauxite deposit at Kanisheeteh, east of Bukan, Iran. *Journal of Geochemical Exploration*, 94, 1-18.

Costa M.L. and Araujo E.S. (1996) - Application of multi-element geochemistry in Au-phosphate-bearing lateritic crusts for identification of their parent rocks. *Journal of Geochemical Exploration*, 57, 257-272.

Crinci J. and Jurkowic I. (1990) - Rare earth elements in Triassic bauxites of Croatia Yugoslavia. *Travaux*, 19, 239-248.

Deer W.A., Howie R.A. and Zussmann J. (1992) - The Rock Forming Minerals. Longman, London, 720 p.

Esmaeili D., Rahimpour-Binab H., Esna-Ashari A. and Kananian A. (2010) - Petrography and geochemistry of the Jajarm karst bauxite ore deposit, NE iran: Implications for source rock material and ore genesis. *Turkish Journal of Earth Sciences*, 19 (2), 267-284.

Feng J.L. (2011) - Trace elements in ferromanganese concretions, gibbsite spots, and the surrounding terra rossa overlying dolomite: Thrie mobilization, redistribution and fractionation. *Journal of Geochemical Exploration,* 108, 99-111.

Fernández-Caliani J. and Cantano M. (2010) - Intensive kaolinization during a lateritic weathering event in southwest Spain mineralogical and geochemical inferences from a relict paleosol. *Catena*, 80, 23-33.

Fleet A.J. (1984) - Aqueous and sedimentary geochemistry of the rare earth elements, in: Henderson, P. (Ed.), Rare earth element geochemistry. Elsevier, pp. 343-373.

Floyd P.A. and Winchester J.A. (1978) - Identification and discrimination of altered and metamorphosed volcanic rocks using immobile chemical elements. *Chemical Geology*, 21, 291-306.

Freyssinet P., Butt C.R.M., Morris R.C. and Piantone P. (2005) - Ore-forming processes related to laterite weathering. *Economic Geology*, 100th Anniversary Volume: 681-721.

Gouveia M.A., Prudencio M.I., Figueiredo M.O., Pereira L.C.J., Waerenborgh J.C., Morgado I., Pena T. and Lopes A. (1993) - Behaviour of REE and other trace and major elements during weathering of granitic rocks, Evora, Portugal. *Chemical Geology,* 107, 293-296.

Grant J.A. (1986) - The isocon diagram-a simple solution to Gresens equation for metasomatic alteration. *Economic Geology*, 81, 1976-1982.

Gresens R.L. (1967) - Composition-volume relationships of metasomatism. *Chemical Geology*, 2, 47-55.

Harnois L. (1988) - The C.I.W. index: A new chemical index of weathering. *Sedimentary Geology,* 23, 1-101.

Kamineni D.C. and Efthekhar-nezad J. (1977) - Mineralogy of the Permian laterite of Northwestern Iran. *Tschermaks Mineralogische und Petrographische Mitteilungen*, 24 (4), 95-204.

Liu X., Wang Q., Deng J., Zhang Q., Sun S. and Meng, J. (2010) - Mineralogical and geochemical investigations of the Dajia Salento-type bauxite deposits, western Guangxi, China. *Journal of Geochemical Exploration*, 105, 137-152.

Ma J., Wei G., Xu Y., Long W. and Sun W. (2007) - Mobilization and re-distribution of major and trace elements during extreme weathering of basalt in Hainan Island, South China. *Geochimica et Cosmochimica Acta*, 71, 3223-3237.

MacLean W.H. and Kranidiotis P. (1987) - Immobile elements as monitors of mass transfer in hydrothermal alteration: Phelps Dodge massive sulfide deposit, Matagami, Quebec. *Economic Geology*, 82, 951-962.

Marques J.J., Schulze D.G., Curi N. and Mertzman, S.A. (2004) - Trace element geochemistry in

Brazilian Cerrado soils. *Geoderma,* 121, 31-43.
Mason B. and Moore C.B. (1982) - Principles of Geochemistry. John Wiley and Sons, 331 p.
Meinhold G. (2010) - Rutile and its applications in earth sciences. *Earth- Science Reviews*, 102, 1-28.
Meyer F.M. (2004) - Availability of bauxite reserves. *Natural Resources Research*, 13, 161-172.
Mondillo N., Balassone G., Boni M. and Rollinson G.G. (2011) - Karst bauxites in the Campania Apennines (southern Italy): a new approach. *Periodico di Mineralogia*, 80 (3), 407-432.
Mongelli G. (2002) - Growth of hematite and boehmite in concretions from ancient karst bauxite: Clue for past climate. *Catena*, 50, 43-51.
Mordberg L.E. (1993) - Patterns of distribution and behavior of trace elements in bauxites. *Chemical Geology,* 107, 241-244.
Mordberg L.E. (1999) - Geochemical evolution of a Devonian diaspore-crandallite-svanbergite-bearing weathering profile in the Middle Timan, Russia. *Journal of Geochemical Exploration*, 66, 35-361.
Mutakyahwa M.K.D., Ikingura J.R. and Mruma A.H. (2003) - Geology and geochemistry of bauxite deposits in Lushoto District, Usambara Mountains, Tanzania. *Journal of African Earth Sciences,* 36, 357-369.
Muzaffer-Karadağ M., Küpeli S., Arýk F., Ayhan A., Zedef V. and Döyen A. (2009) - Rare earth element (REE) geochemistry and genetic implications of the Mortaş bauxite deposit (Seydişehir/Konya-Southern Turkey). *Chemie der Erde-Geochemistry,* 69, 143-159.
Nesbitt H.W. and Wilson R.E. (1992) - Recent chemical weathering basalts. *American Journal Earth Science,* 29, 740-777.
Nesbitt H.W. and Young G.M. (1982) - Early Proterozoic climates and plate motions inferred from major element chemistry of lutites. *Nature,* 279, 715-717.
Özlü N. (1983) - Trace element contents of karst bauxites and their parent rocks in the Mediterranean belt. *Mineralium Deposita*, 18, 469-476.
Retallack G.J. (2010) - Lateritization and bauxitization events. *Economic Geology*, 105, 655-667.
Schellmann W. (1982) - Eine neue Laterit definition. *Geologisches Jahrbuch - Reihe D*, 58, 31-47.
Schroll E. and Sauer D. (1968) - Beitrag zur Geochemie von Titan, Chrom, Nikel, Cobalt, Vanadium und Molibdan in Bauxitischen gestermen und problem der stofflichen herkunft des Aluminiums. *Travaux de ICSOBA*, 5, 83-96.
Schwertmann U. and Pfab G. (1994) - Structural vanadium in synthetic goethite. Geochimica et *Cosmochimica Acta*, 58, 4349-4352.
Shaw D.M. (1964) - Interprétation géochemique des éléments en traces dans les roches cristallines. Masson et Cie, Paris.
Sparks D.L. (1995) - Environmental soil chemistry. New York, Academic Press.
Tardy Y. and Nahon D.B. (1985) - Geochemistry of laterites, Stability of Al-goethite, Al-hematite and Fe^{3+}-kaolinite in bauxites and ferricretes: An approach to the mechanism of concretion formation. *American Journal of Science*, 285, 865-903.
Tripathi K.J. and Rajamani V. (2007) - Geochemistry and origin of ferruginous nodules in weathered granodioritic gneisses, Mysore plateau, southern India. *Geochimica et Cosmochimica Acta*, 71(7), 1674-1688.
Valeton I. (1972) - Bauxites. Elsevier, 226 p.
Vaziri-Moghaddam H., Kimiagari M. and Tehrani A. (2006) - Depositional environment and sequence stratigraphy of the Oligo-Miocene Asmari Formation in SW Iran. *Facies*, 52, 41-51.
Wang Q., Deng J., Liu X., Zhang Q., Sun S., Jiang C. and Zhou F. (2010) - Discovery of the REE minerals and its geological significance in the Quyang bauxite deposit, West Guangxi, China. *Journal of Asian Earth Sciences,* 39, 701-712.
Wilson M.J. (1994) - Clay Mineralogy: spectroscopic and chemical determinative methods. Chapman and Hall.
Zarasvandi A., Charchi A., Carranza E.J.M. and Alizadeh B. (2008) - Karst bauxite deposits in the Zagros Mountain Belt, Iran. *Ore Geology Reviews,* 3, 521-532.
Zarasvandi A., Zamanian H. and Hejazi, E. (2010) - Immobile elements and mass changes geochemistry at Sar-Faryab bauxite deposit, Zagros Mountains, Iran. *Journal of Geochemical Exploration,* 107, 77-85.

Submitted, September 2012 - Accepted, January 2013